3D Elastic Registration of Vessel Structures from IVUS Data on Biplane Angiography[1]

Benoit Godbout, M Ing, Jacques A. de Guise, PhD, Gilles Soulez, MD, Guy Cloutier, PhD

Rationale and Objectives. Planar angiograms and intravascular ultrasound (IVUS) imaging provide important insight for the evaluation of atherosclerotic diseases and blood flow abnormalities. The construction of realistic three-dimensional models is essential to efficiently follow the progression of arterial plaque. This requires an explicit localization of IVUS frames from angiograms. Because of the difficulties encountered when trying to track the position of an IVUS transducer, we propose an elastic registration approach that relies on a virtual catheter path.

Materials and Methods. Deformable surface models of the lumen and external wall are constructed from segmented IVUS contours. A crude registration is obtained using a three-dimensional vessel centerline, reconstructed from two calibrated angiograms. Robust optimization of the virtual catheter path, position, absolute orientation, and regulation of the external wall shape is performed until near-perfect alignment of the back-projected silhouettes on image edges is reached.

Results. Visual assessment of the reconstructed vessels showed a good superposition of virtual models on the angiograms. We measured a 0.4-mm residual error value. A preliminary study of convergence properties on 15 datasets showed that initial absolute orientation may affect the solution. However, for follow-ups, coherent solutions were found among datasets.

Conclusion. The advantages of the virtual catheter path approach are demonstrated. Future work will look at ways to single out the true solution with a better use of the available information in both modalities and additional validation studies on improved datasets.

Key Words. Biplane angiography; intravascular ultrasound; multimodal image registration; peripheral arteries.

The construction of three-dimensional (3D) realistic artery models is essential for studying atherosclerotic disease and blood-flow abnormalities. Planar angiograms remain the prevalent imaging technique during endovascular interventions. However, there are serious limitations in working with a single planar projection when precise measurements are required. The limited spatial resolution and the cost associated with 3D imaging techniques such as computed tomography angiography (CTA), magnetic resonance angiograpy (MRA), or rotational angiography can also be a serious drawback.

Intravascular ultrasound (IVUS) is a powerful imaging technique for evaluating vessel cross-sections. High-resolution images show the shape and size of the lumen, plaque, and vessel wall. By performing a constant-speed pullback inside the vessel, a tomographic-like reconstruction of a straightened vessel can be obtained. However, without explicit localization of IVUS slices, 3D measurements are distorted.

Some authors have worked on data fusion of IVUS and angiography (1–3). The main research areas are angiographic system calibration, catheter path segmentation,

Acad Radiol 2005; 12:10–16

[1] From the Laboratoire de Recherche en Imagerie et Orthopédie, CRCHUM, 1560 Sherbooke Est (Y-1615), Montréal, H2L-4M1, Canada (B.G., J.A.d.G.), École de Technologie Supérieure, Montréal, Canada (B.G., J.A.d.G.), Département de Radiologié, CHUM, Montréal, Canada (G.S.), Laboratoire de Biorhéologie et Ultrasonographie Médicale, Montréal, Canada (G.C.). Supported by grants from the Canadian Institute of Health Research (G.C., G.S., #MOP-53244), Valorisation-Recherche Québec (group grants #2200-094 and #2200-003), and National Science and Engineering Council of Canada (J.A.d.G., #107998-99). Drs. J.A. de Guise, G. Soulez, and G. Cloutier are, respectively, recipients of a Canada Research Chair, a clinical research scholarship award from the Fonds de Recherche en Santé du Québec (FRSQ), and of a National Scientist Award, also from FRSQ. **Address correspondence to** B.G. benoit.godbout@etsmtl.ca or G.C. guy.cloutier@umontreal.ca

doi:10.1016/j.acra.2004.10.058

biplanar curve reconstruction, and absolute orientation determination. These techniques have a number of disadvantages in a clinical setting. For instance, because most angiography rooms do not have biplane systems or complex calibration objects, the images must be taken sequentially. Moreover, video images often show poor quality and image synchronization requires specialized hardware. As a result, segmenting and following the 3D path of an IVUS transducer or guide wire can be difficult.

We proposed a novel technique (4) to elastically register a 3D deformable vessel model from two-dimensional angiographic images without explicit knowledge of the catheter path. A simple angiographic image calibration technique using a radiopaque ruler attached to the patient was used. A tubular parametric model of the vessel, constructed from IVUS datasets, was elastically registered to recover the catheter path and absolute orientation. The method has now been improved to include some shape regulation and pullback position adjustments.

This work aims to exploit images from an existing clinical protocol. Angiograms and IVUS imaging were used to investigate the changes in stenosis diameter and plaque distribution over femoral arteries after angioplasty. The main objective was to better visualize and quantify the plaque distribution around the vessel using our registration method with the existing images.

The long-term clinical goal is to provide a thorough evaluation tool for following the progression/regression of the disease before and after therapeutic interventions. Other potential uses of the models include computational-fluid-dynamics simulations and realistic phantom construction via rapid prototyping technologies (5).

MATERIALS AND METHODS

To follow the changes in plaque distribution, true 3D representations of the structures of interest, namely the lumen and external vessel border, must be obtained at different intervals. For this purpose, two plane angiography images (Toshiba DFP-2000, Japan) and an IVUS pullback (Jomed In-Vision, The Netherlands) were acquired before angioplasty of the superficial femoral artery, just after angioplasty and during a follow-up visit 1 year later. The prospective double blinded clinical protocol was approved by the ethical committee of University of Montreal Hospital.

The description of the method is organized as follows: the first section explains the calibration and reconstruction method of the vessel centerline from biplane angiography. A description of the model construction from IVUS pullback slices and elastic deformation follows in the second section.

The third and fourth sections introduce the main contribution of this work. A crude registration is first obtained using the reconstructed centerline from the angiograms. The virtual catheter path is then elastically registered to achieve a near perfect alignment of the back-projected silhouettes on image contours. The virtual catheter path parameters (start position, pullback speed, and absolute orientation) are optimized simultaneously.

Biplane Angiography

For every dataset, two angiograms are taken. A coronal view is acquired first. A second view is taken after rotating the C-arm around the patient by 30°. A radiopaque ruler, taped to the patient's leg, is included for calibration purposes. Images are printed on film and later scanned using a Vidar DiagnosticPro film digitizer. A grid of radiopaque markers is used to acquire, compute, and correct, by means of high-order polynomials, the distortions induced by the amplifier (6).

Three-dimensional reconstruction and registration require calibration parameters. The field of view, view angle, and distance from source to amplifier are set to C-arm control values. The exact position of the rotation axis between views are computed from two positions on the radiopaque ruler by including the stereo correspondence and fixed length constraints in the projective equations. The calibration values are expressed in a homogenous matrix form.

A symmetry-seeking active contour method inspired by Terzopulos et al. (7) and Godbout et al. (8) is used to segment the lumen centerline. Linear interpolation between 3 or 4 manually defined points on the centerline provides an initial guess. The centerline contour then deforms itself by seeking two opposite image gradient maxima while regularizing its stiffness and width.

From the two-dimensional centerlines, one for each view, ray intersections and epipolar geometry equations (6) can be used to reconstruct a 3D vessel centerline. Figure 1 illustrates the calibration and reconstruction process. The 3D centerline is a rough estimate of the 3D shape of the lumen. To recover the exact shape, the axial cross-section of the vessel must be known. IVUS imaging offers this information.

Model Construction

Each IVUS dataset is made of 600 to 1,300 cross-sectional slices of the vessel recorded from a 20 MHz transducer at the tip of the catheter. The lumen and external

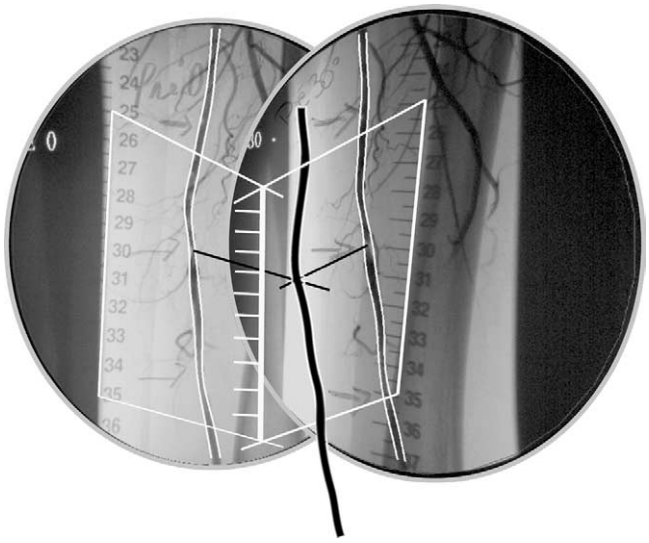

Figure 1. Three-dimensional centerline of the lumen reconstructed by epipolar geometry from calibrated (with a radiopaque ruler) biplane angiography views.

vessel wall are efficiently segmented using a semiautomatic fast-marching method (9). Assuming a constant pullback speed during the acquisition at 0.1 mm/frame, contours are positioned in space to obtain a geometric representation of the lumen and external border of the media, centered on a straightened catheter path. A tubular third-degree parametric B-spline surface is least-square fitted to the contours with an approximate 0.4 mm distance between control points. Figure 2 shows segmented IVUS frames and the resulting tube model.

A single central B-spline curve C controls the deformation of the parametric B-spline tubes by transforming the surface control points. We used the relative twist model of Wahle et al (1). This model, built on torsion-free Frenest frames, was validated for small flexion angles and should hold for femoral artery reconstruction.

In this framework, the central curve is subdivided in M equidistant points, M being the number of contours of the tube along the axis. The reference frames align themselves to the tangents of the central curve (Z axis). To impose an absolute orientation around the control curve, an arbitrary normal vector (X axis) is assigned to the first frame. The cross-product of Z and X defines a corresponding binormal vector (Y axis). All other frames are computed with successive torsion free rotations to align the Z axes. The lumen and external wall surface's control points are transformed using the computed frames along the central curve. Figure 2 illustrates the model construction and the deformation of parametric B-spline tubes along the control curve.

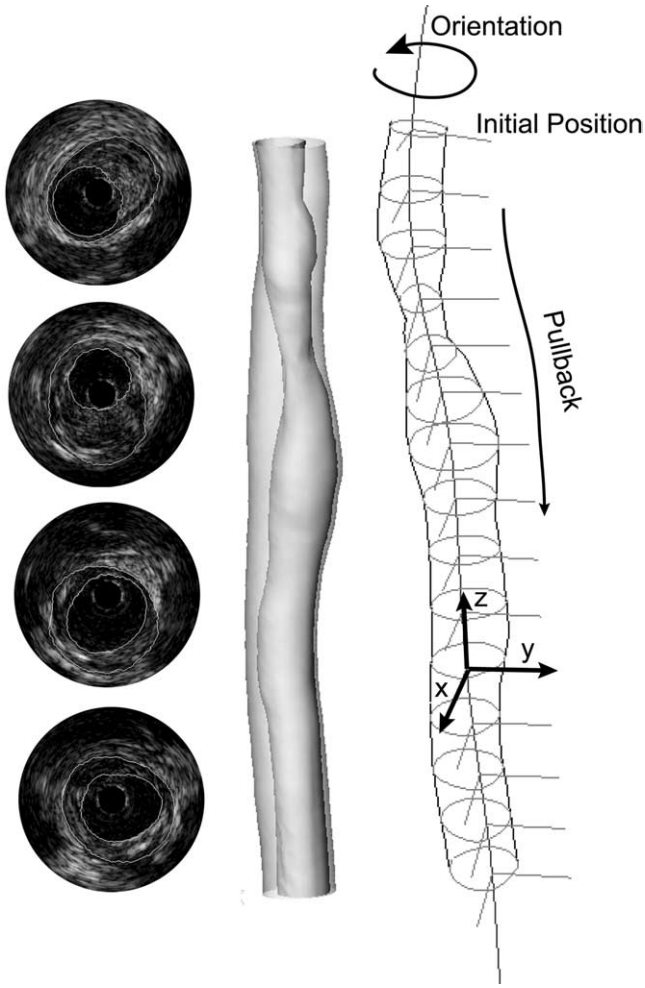

Figure 2. Contours extracted from intravascular ultrasound images (left). The tubular model (center) is deformed along a B-spline control curve (right).

By imposing the control curve to mimic the catheter path during the pullback, a realistic surface model of the lumen and vessel wall can be obtained. Whereas other authors (1–3) use an explicit reconstruction of the catheter to achieve the reconstruction, this work uses a virtual catheter path.

Initial Registration

The reconstructed 3D centerline obtained from the angiographic views supplies an initial estimate of the catheter path. For the crude registration, the tube's control curve is bound to slide along this centerline. The absolute orientation and pullback length can also be adjusted.

Silhouette contours are defined as the external boundaries of the back-projected model, when seen in the calibrated angiographic view. A boundary usually appears in a two-dimensional view when a ray casting from the sur-

face point towards the focal point (in this case the x-ray source position) is tangent to the surface. Formally, the silhouette contours are found at the zero crossings of the ray direction and surface normal vectors dot product. They could be extracted from any surface model and back-projected on a calibrated image.

A user interface was developed to give immediate feedback on the reconstruction quality at interactive rate using silhouette and other rendering strategies. Silhouettes can be manually registered to align a stenosis on both views. An approximate superposition is sufficient at this point.

A width-map method for automating the crude registration was previously described elsewhere (4). It relied on the cross-correlation of visible width between the model and images to find an initial pullback position and the absolute orientation. The reliability of the method is still under evaluation. In this work, manual positioning with visual feedback was used instead.

At this point, we have an estimate of the catheter path start and stop positions as well as an absolute orientation. The next step is to refine the catheter path with an automated registration of the vessel model on the images.

Elastic Registration

We propose here a novel method to precisely register vessel models into angiograms. Deformable models have been used widely (10) in the medical imaging community since Kass et al. (11) introduced the snake model. Those methods are based on the minimization of an energy function. An external energy or image likelihood function tends to overlay the silhouette contours on image edges. To regulate the process, an internal energy or shape function is introduced. For our method, the expected vessel model is obtained by solving the following equation:

$$\arg\min_{C,R}\left(\sum_i d_i^2 + \left(\sum_k \frac{\partial^2}{\partial v^2}\beta_k(v)\cdot(C_k + E_k)\right)^2\right) \quad (1)$$

where the degrees of freedom are the control points C_k of the B-spline control curve C and the absolute orientation R. The internal energy function that minimizes the vessel curvature is the squared second derivative of a B-spline function β. Because of the plaque deposits and pulsatile nature of lower limb arterial flow, the catheter path and lumen centerline oscillate from side to side during the pullback, whereas the external vessel wall boundary stays straight. A centerline offset E_k is added to the control curve to compute the vessel wall centerline curvature.

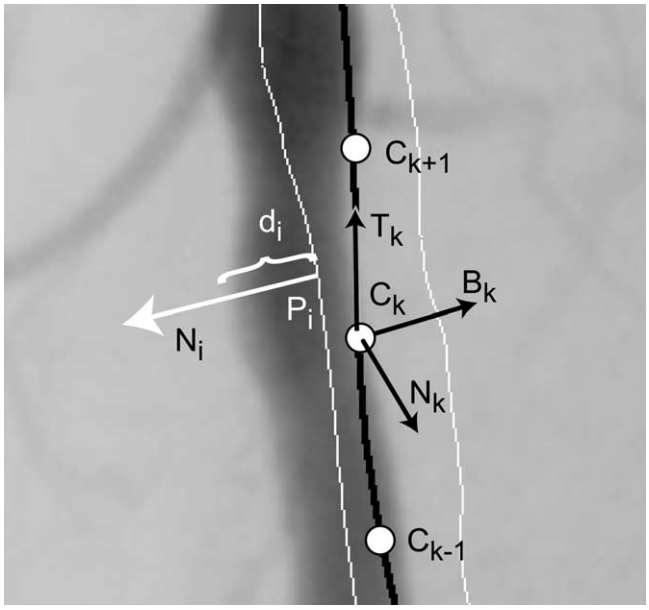

Figure 3. Silhouette point (Pi) distance (di) minimization along its normal (Ni) by moving control points (Ck) in normal (Nk), binormal (Bk), and tangent (Tk) directions.

The sum of squared distances d_i between the current model's silhouette contours and matching image edges acts as an external energy function. The search for potential edge locations in the two calibrated images is done along profiles on both sides of back-projected silhouette contours. For every silhouette points, a single 3D distance to the best oriented image edge is kept, as illustrated in Fig. 3. A bicubic spline image representation proposed by Unser et al. (12) allows quadratic sampling of the image gradient amplitude and direction.

A linearized displacement field optimization strategy efficiently solves Eq 1. The algorithm defines a set of linear equations that relate the displacement of a silhouette point P_i along its 3D normal N_i to the change in the parameters for the current back-projected model. For control points C_k, translations $t_{n,k}$, $t_{b,k}$ are allowed along their frame's normal N_k and binormal B_k directions. The corresponding field equation is:

$$d_i = \sum \beta_k(v_i)\cdot\left[\left(\vec{N}_k\cdot\vec{N}_i\right)\cdot t_{n,k} + \left(\vec{B}_k\cdot\vec{N}_i\right)\cdot t_{b,k}\right] \quad (2)$$

where B-spline weights β_k of silhouette points modulate the effect of each control point on the displacement. Global displacement fields are added to the equation for the translation along the curve's tangent t_t, the length change of the curve l_o, and a rotation around the curve r_o giving the following displacements fields:

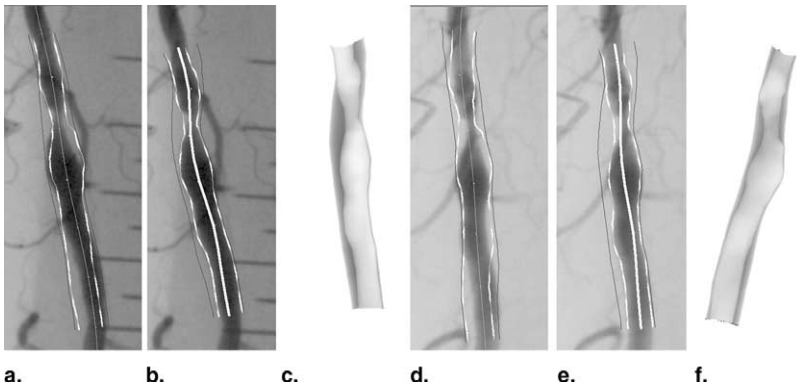

Figure 4. Example of reconstruction. Initial (a,d) and registered (b,e) silhouettes as well as reconstructed vessels (c,f) are shown for the coronal (a,b,c), 30° view (d,e), and lateral (f) views.

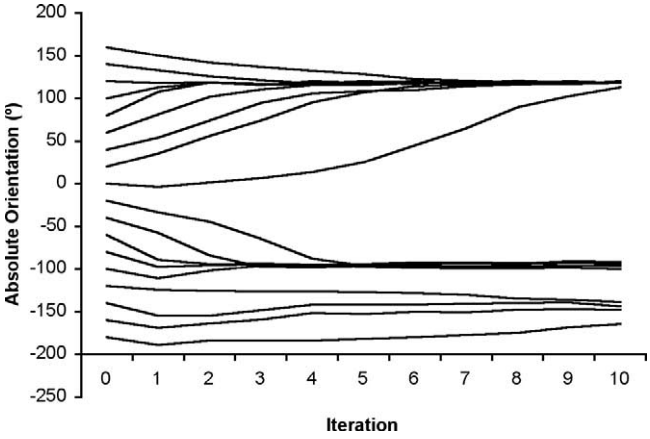

Figure 5. Changes in intravascular ultrasound frames absolute orientation during iterative registration for different initial values. Two clear optimal solutions and a few outliers are found.

$$d_i = \vec{T}_{\mathrm{k}} \cdot \vec{N}_{\mathrm{i}} \cdot t_t + (v_i - 0.5) \cdot \vec{T}_{\mathrm{k}} \cdot \vec{N}_{\mathrm{i}} \cdot l_o + (\vec{P}_{\mathrm{i}} \times \vec{N}_{\mathrm{i}})_t \cdot r_o \quad (3)$$

These parameters adjust the start position, pullback speed and absolute orientation. The combination of Eqs 2 and 3 describes a first set of M equations where M is the total number of silhouette points on both angiograms. A second set of N equations stands for the internal energy term, N being the number of control points of the control curve:

$$\frac{\partial^2}{\partial v^2} \beta_k(v) \cdot (C_k + E_k) = -\sum_k \frac{\partial^2}{\partial v^2} \beta_k(v) \cdot \left[\vec{N}_{\mathrm{k}} \cdot t_{n,k} + \vec{B}_{\mathrm{k}} \cdot t_{b,k} \right] \quad (4)$$

The solution of Eq 4 amounts to control point displacement needed to cancel the second derivative of the external vessel wall centerline. The right side of both equation sets (2 and 3; 4) is put in matrix form giving $M+N$ equations with $2*N + 3$ unknowns. A typical equation system would have 12 control points and 1,000 silhouette points.

Solving the linear regression with robust least-squares (13) reduces the impact of false contour matching on the results. Outliers are gradually penalized, with the iteratively reweighted least-squares algorithm to minimize the pulling effect they would have with classic least-squares. The control curve is updated with:

$$C'_{\mathrm{k}} = C_k + t_{n,k} \cdot \vec{N}_k + t_{b,k} \cdot \vec{B}_{\mathrm{k}} + (t_t + (v_k - 0.5) \cdot l_o) \cdot \vec{T}_k \quad (5)$$

and the absolute orientation is given by:

$$R' = R + r_o \quad (6)$$

After a few iterative updates of the control curve, the virtual catheter path should mimic reality in reconstruction space providing a realistic representation of vessel geometry.

RESULTS

The whole method was integrated into a C++ software library. The software interface inputs the biplane angiograms and the segmented IVUS contours. It allows interactive reconstruction and visualization of the model back-projections from any viewpoints. Models are exported as virtual reality modeling language (VRML) or initial graphics exchange specification (IGES) file format to be used as input for computational-fluid-dynamics, finite element analysis or 3D measurement software.

The whole procedure, including the user delineation of the ruler and initial vessel path as well as calibration,

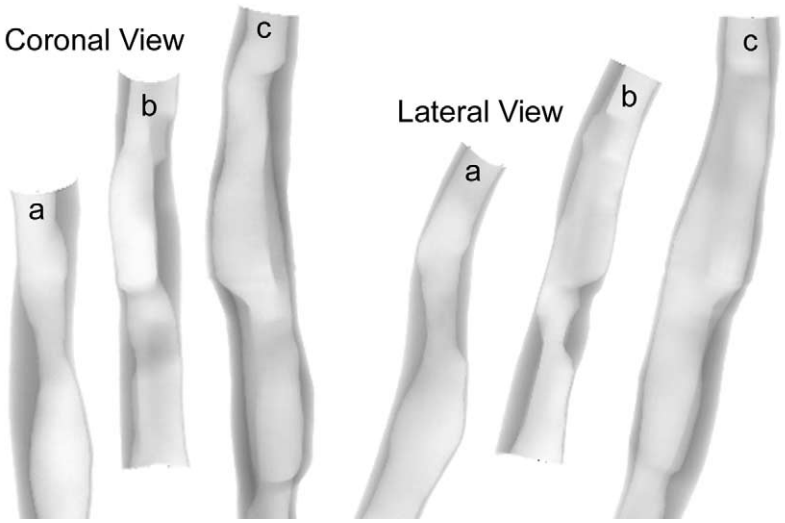

Figure 6. Reconstructed femoral artery sections, aligned in coronal and lateral views for the preangioplasty (a), postangioplasty (b), and 1-year follow-up (c) datasets. The stenosis are aligned even if pullback endpoints differ.

takes less than 1 minute to perform. Depending on the pullback length and image resolution, 3 to 10 seconds are needed to compute the fine registration on an MS Windows–based Pentium III-1GHz. Unsatisfying initialization data or results can be manually adjusted. The number of iterations is the only parameter. Typically, 10 iterations are sufficient to converge to an adequate solution.

The validation study is based mostly on the visual assessment of the algorithm convergence on real data. Five artery segments belonging to three patients were reconstructed from preangioplasty, postangioplasty, and 1-year follow-up datasets. Some follow-up reconstructions were discarded because of short or misaligned IVUS pullbacks.

Figure 4 shows a typical result. Initial and final silhouettes and virtual catheter path are shown on both views. The reconstructed plaque is ray-traced in the coronal and lateral views to appreciate its thickness. The alignment of the stenosis and other features seems adequate after the elastic registration. The overall root-mean-squared residual distance is approximately 0.4 mm with a mean error value of −0.1 mm which implies that the angiogram contours are slightly smaller than the models.

The convergence and reproducibility characteristics of the algorithm are also studied. The main source of variability, besides proper initial alignment, is the initial value of absolute orientation. Figure 5 shows the evolution of the absolute orientation in the course of iterations for the reconstruction of Fig. 4. Initial orientations varied from −180° to 160° with steps of 20°. The final orientation values present two clear minima and a few outliers. The most consistent is at 120°. We observed that other registered models present a similar behavior.

Figure 6 shows how the plaque volume changed after angioplasty for the three aligned datasets of an artery segment. The initial absolute orientations are chosen to generate coherent solutions among datasets.

DISCUSSION

The visual assessment and residual distance are generally quite good. However, we found that when many solutions coexist, the energy values could not determine a winner. A 30° angle between views creates a lot of redundancy in the projected shape. Because of symmetry, at least two opposite energy minima are expected. We find such minima in all cases. Choosing a larger angle between views or even adding a third view would refine the solution.

The offset in the mean residue is small at −0.1 mm, but is always negative. It could be caused by some segmentation or calibration artifacts in the IVUS or angiographic images. The exact cause could not be pinpointed without using phantoms or other means.

To locate the pullback position, the external energy term is mainly influenced by the projected width discrepancies along the vessel. For the absolute orientation, the regulation term, which uses the external wall as a reference, plays an important role in defining an optimal solution. Thus the reconstruction quality depends on asymmetrical plaque deposits in otherwise straight arteries.

For position and absolute orientation, a cylindrical vessel is the worst case scenario for convergence. Luckily, these cases have little clinical relevance. Long pullbacks in significantly affected arteries have a better defined solution. However, a case had to be discarded because of poor angiograms and IVUS image quality caused by a near-complete obstruction of the vessel.

When using this method for follow-ups, we rely on coherence of the plaque deposits to help us select an optimal solution. The plaque distribution from an earlier reconstruction can be visualized after the prior vessel model is rigidly registered to the angiographic data. The results are satisfying when using this approach. The process could be further automated with a concurrent space-time registration approach to get a consistent deformation of the plaque volume among datasets.

In Fig. 6, we clearly see on the lateral view that a residual stenosis is present in the postangioplasty lumen. This shows the relevance of such reconstructions during an intervention. The stenosis seems to have regressed at the 1-year follow-up. More work is needed to validate those results.

CONCLUSION

A new elastic registration technique for 3D lumen and artery wall reconstruction from IVUS and biplane angiography data was proposed. The catheter path and orientation, as well as the pullback start and stop positions, were found by minimizing the distance between silhouettes of the back-projected lumen and angiographic image contours. Results on real data were promising and showed the convergence of the algorithm.

Although some ambiguities remained in the results, the method clearly presents advantages over previous ones when the catheter is poorly visible. Our future work will look at ways to lift the ambiguities and single out the true solution. Further validation will be conducted. In the absence of a gold standard, using cross-validation with views taken from different angles will give a better assessment of the 3D path reconstruction quality. Synthetic images and radiologic phantom images (5) could also be used for validation purposes.

We found that a fusion approach, using the full potential of both modalities on evolving datasets, can lead to a better understanding of atherosclerotic disease. More tightly integrated IVUS and angiography segmentation techniques could solve the registration problem. Examples are using collateral arteries in angiographic and IVUS image space to constrain the absolute orientation or using plaque displacement analysis for follow-up studies.

Full automation and speed optimization is an important issue and will be considered for future enhancements. The method could easily be adapted to include space-time catheter path registration. Cardiac imaging and real-time reconstruction for computer assisted intervention are promising applications of this work.

REFERENCES

1. Wahle A, Prause G, DeJong S, et al. Geometrically correct 3-D reconstruction of intravascular ultrasound images by fusion with bi-plane angiography—methods and validation. IEEE Trans Med Imag 1999; 18: 686–699.
2. Slager CJ, Wentzel JJ, Schuurbiers JC. True 3-dimensional reconstruction of coronary arteries in patients by fusion of angiography and IVUS (ANGUS) and its quantitative validation. Circulation 2000; 102:511–516.
3. Rotger D, Radeva P, Mauri J, et al. Internal and external coronary vessel images registration. In: Escrig MT, ed. Proceedings of CCIA, LNAI 2504. Berlin: Springer-Verlag, 2002; 408–418.
4. Godbout B, de Guise JA, Soulez G, et al. 3D elastic registration of vessel lumen from IVUS data on biplane angiography. In: Ellis R, Peters TM eds. Proceedings of the 6th International MICCAI Conference (Montreal). LNCS 2878. Berlin: Springer-Verlag, 2003;303–310.
5. Cloutier G, Soulez G, Quanadli SD, et al. A multimodality vascular imaging phantom with fiducial markers visible in DSA, CTA, MRA, and ultrasound. Med Phys 2004; 31:1424–1433.
6. Cañero C, Vilariño F, Mauri J, et al. Predictive (un)distortion model and 3D reconstruction by biplane snakes. IEEE Trans Med Imag 2002; 19: 1188–1201.
7. Terzopoulos D, Witkin A, Kass M. Symmetry—seeking models for 3D object reconstruction. Int J Comput Vision 1987; 1:211–221.
8. Godbout B, Kauffmann C, de Guise JA. A simple 2D active contour model to segment non-convex objects in 3D images. In: Cheriet M, Yang YH, eds. Proceedings of Vision Interface. Vancouver, Canada: 1998; 456–464.
9. Roy-Cardinal MH, Meunier J, Soulez G, et al. Intravascular ultrasound image segmentation: a fast-marching method. In: Ellis R, Peters TM, eds. Proceedings of the 6th International MICCAI Conference (Montreal). LNCS 2879. Berlin: Springer-Verlag, 2003; 432–439.
10. McInerney T, Terzopoulos D. Deformable models in medical image analysis: A survey. Med Image Anal 1996;1:91–108.
11. Kass M, Witkin A, Terzopoulos D. Snakes. Active contour models. Int J Comput Vision 1998; 1:321–31.
12. Unser M, Aldroubi A, Eden M. B-spline signal processing: Part II—efficient design and applications. IEEE Trans Signal Proc 1993;41:834–848.
13. Holland PW, Welsch RE. Robust regression using iteratively reweighted least-squares. Commun Stat Theory Meth 1977; A6:813–827.